Dynamical Mechanical Thermal Analysis of Shape Memory Polymers

Pauline Butaud, Morvan Ouisse, Kévin Jaboviste, Vincent Placet and Emmanuel Foltête

Abstract This chapter is dedicated to the Dynamical Mechanical Thermal Analysis of Shape Memory Polymers. Temperature obviously plays a major role in the mechanical properties of these materials, hence the understanding of the physical phenomena driving the shape memory effect is of first importance for the design of practical applications in which Shape Memory Polymers are used. The Shape Memory effect being closely related to the viscoelastic behavior of the polymer, it is important to properly describe it with appropriate tools. The objective of this chapter is to describe characterization methods, models and parameters identification techniques that can be easily used for the description of the thermo-mechanical behavior of SMPs. The associated models can easily be implemented in finite element codes for time or frequency domain simulations. The experimental results and all numerical values of the models are provided for three Shape Memory Polymers: the tBA/PEGDMA and a Vitrimer, which can easily be manufactured according to the data provided in open literature, and a Shape Memory Polymer filament for 3D printing, which is available on the shelf.

1 Introduction

As all polymers, Shape Memory Polymers (SMPs) exhibit a strong viscoelastic behavior. The stable rubbery and glassy states play a major role in the Shape Memory effect, which is associated to a fast transitions between these states with a large elasticity gap, inducing high loss factor values at glass transition [50, 2]. The typical values of the loss factor which are reported in SMP-related open literature typicaly vary between 0.5 [4] and more than 2.5 [39, 7], most of them being between 1 and 2 [49, 53, 20, 8]. These qualitatively high values of loss factor must be considered for

All authors

University of Bourgogne Franche-Comté - FEMTO-ST Department of Applied Mechanics, 24 rue de l'Epitaphe - 25000 Besançon, e-mail: morvan.ouisse@femto-st.fr

practical applications since they can have strong impact on the efficiency and the behavior of the SMP-based devices. For applications in which only static phenomena are involved, the intrinsic losses may be neglected but as soon as dynamical phenomena contribute to the mechanical response, viscoelastic effects must be considered. This has been highlighted for years now, and numerous works can be found in the literature that present models of the shape memory effect based on rate-dependent viscoelastic models [11, 34, 17, 56, 21, 55, 32]. Recently, these materials have been identified as able to play a major role in damping-related applications, thanks to the high damping capacities associated to the glass transition [13]. In these applications, the shape memory material acts as a classical passive damping treatment, which is known to be a reliable, low cost and robust solution for vibration control [22, 40], whose damping and stiffness can be tuned by a temperature control [6]. The polymer layer is classicaly used as a core in a multilayered composite, in order to enhance the shear effects in the material, leading to high damping performances. Many articles have been published on composite structures embedding viscoelastic materials to damp vibrations [24, 1]. The design optimization of multilayers structures has particularly been investigated [33, 31, 3, 19] by varying the thickness of the viscoelastic layer, the fiber orientation or the aspect ratio of the structure. When dealing with these materials, it is important to precisely describe the behavior of interest with adequate models based on confident parameters. The most usual way to obtain the viscoelastic mechanical properties of a polymer is the Dynamic Mechanical Analysis (DMA), also called Dynamical Mechanical Thermal Analysis (DMTA), which consists in conducting mechanical tests on a small frequency band and a large temperature range [16, 48, 25]. By using laws as Williams-Landel-Ferry (WLF) law [51] or Arrhenius law [45], in a Time-Temperature Superposition (TTS) model, DMA measurements are used in order to obtain the mechanical behavior of the polymer on a large band of frequencies and temperatures. The extrapolated properties obtained can then be used to design composite structures. Even if some limitations of this apparatus have been reported, (effect of the instrument compliance [26], of the specimen dimensions [15] or even of the chosen TTS model [8]), and despite of the fact that viscoelastic properties are often obtained only for a specific loading mode, DMA remains a confident way to obtain a description of the behavior which is valid for different loading modes, for different scales, on wide temperature and frequency ranges, even for Shape Memory Polymers [7]. Among others, these materials are very good candidates for temperature-controlled damping devices [6, 5].

In this chapter, original results are presented for three Shape Memory Polymers: the tBA/PEGDMA and the Vitrimer, which can easily be manufactured according to the data provided in open literature, and a Shape Memory Polymer filament for 3D printer, which is available on the shelf. For each of these materials, DMA results are performed by varying frequency and temperature, the TTS is checked and a corresponding model is described. Finally, a viscoelastic model (Generalized Maxwell Model) is identified in order to describe the behavior of the material on a wide frequency and temperature ranges. All numerical values of the models are provided in order that readers can use the data in their work.

The chapter is organized as follows: section 2 describes the three materials used in this work, section 3 presents the DMA apparatus and protocol, section 4 describes the viscoelastic and TTS models, and section 5 provides all the results.

2 Materials

In this section, the three materials considered in this chapter are presented.

2.1 tBA/PEGDMA

The tBA/PEGDMA is a Shape Memory Polymer which has been originally studied by Srivastava et al. [47]. This material is used in this work, based on samples elaborated in FEMTO-ST Institute in the Department of Applied Mechanics in accordance with the procedure described in Yakacki et al. [54]. The chemicals components were provided by Sigma-Aldrich and used as received and without purification. The shape memory polymer was synthesized by manually mixing 95 wt% of the monomer tert-Butyl Acrylate (tBA), with 5 wt% of cross-linking agent poly(ethylene glycol) dimethacrylate (PEGDMA) (with a typical molecular weight Mn=550 g/mol). The photo-initiator, 2.2-dimethoxy-2-phenylacetophenone (DMPA), was added to the solution at a concentration of 0.5 wt% of the total weight. The liquid mixture was then injected between two glass slides. A plastic seal was used as a spacer to ensure constant thickness. The polymerization was initiated by exposing the solution to UV light for 10 min and was completed by heating the polymer at 90°C for 1 h. The produced plates were machined whenever necessary for the execution of the mechanical tests.

The tBA/PEGDMA is a thermoset amorphous polymer. A DSC analysis has highlighted the absence of crystallite and full cross-linking of the polymer. Moreover, optical imaging analyses have not shown any polymer heterogeneity. Finally, it should be emphasised that the tBA/PEGDMA is thermo-rheologically simple, as mentioned in Butaud et al. [7]. The mass density of the tBA/PEGDMA is $\rho = 1000$ kg/m^3 (determined by pycnometer). The Poisson's ratio of the tBA/-PEGDMA, determined during quasi-static tests (10^{-4} Hz) at room temperature [7], is $\nu = 0.37$.

2.2 SMP filament

The shape memory polymer filament was provided from SMP Technologies Inc. This polymer is available on the shelf for 3D printing. The filament was used as received and without any printing to avoid structural aspects in the evaluation of the

mechanical properties. The SMP filament is a thermoplastic polymer with a mass density of 1260 kg/m^3 (determined by measuring the sample's mass and volume). This material may be used in most of FDM-based 3D printers to obtain the shapes of interest.

2.3 Vitrimer

The third shape memory polymer studied in this paper is a vitrimer. The vitrimer has been developed by Ludwik Leibler [29]. The hard networks is tested in this work. The material was elaborated at the FEMTOST Institute in the Department of Applied Mechanics in accordance to the procedure described in Montarnal et al. [36]. The chemicals were provided from Sigma-Aldrich and used as received and without any purification. The vitrimer was synthesized by reaction of the diglycidyl ether of bisphenol A (DGEBA) with glutaric anhydride with epoxy/acyl 1:1 in the presence of 5 mol% zinc acetyl acetonate [Zn(acac)2]. The reaction mixture was homogenized with mechanical stirring at 140°Cuntil phase miscibility. The liquid mixture was then molded in plate (210×300×20 mm^3) and the polymerization was performed in a thermal chamber at 140°C for 12 h. The produced plates were machined whenever necessary for the execution of the mechanical tests. The mass density of this hard networks is 1290 kg/m^3 (determined by measuring the sample's mass and volume).

3 Dynamical Mechanical Thermal Analysis

3.1 tBA/PEGDMA

Samples are cut to $29 \times 6 \times 3$ mm. Viscoelastic properties are measured using a Metravib DMA50 apparatus at temperatures varying by 5°C steps (near the glass transition temperature) or 10°C steps (far from the glass transition) at heating rate of 2°C/min, between 30°C and 90°C. The frequency of the excitation varies from 0.1 Hz to 180 Hz. A sinusoidal tensile displacement is applied on the sample with a peak-to-peak amplitude of 10 μm allowing to ensure a linear viscoelastic behavior.

3.2 SMP filament

A Metravib DMA300+ apparatus is used at temperatures varying by 5°C steps at heating rate of 2°C/min, between 33°C and 83°C. The temperature was stabilized during 1 minute before each measurement to ensure a homogeneous temperature

inside the specimen. Specimen's shape is cylindrical, with a diameter of 1.75 mm. The length is cut to 6 mm between the jaws. The frequency of the excitation varies from 0.1 Hz to 180 Hz. A sinusoidal tensile displacement is applied on the sample with a peak-to-peak amplitude of 5 μm allowing to ensure a linear viscoelastic behavior.

3.3 Vitrimer

Viscoelastic properties are measured using a Bose Electroforce 3200 apparatus in isothermal conditions at temperatures varying by 5°C steps at heating rate of 3°C/min, between 36°C and 102°C. The temperature was stabilized during 2 minutes before each measurement to ensure a homogeneous temperature inside the specimen. The temperature was measured by using a thermocouple placed in a reference sample located in the heating chamber close to the tested specimen. The frequency of the excitation varies from 0.01 *Hz* to 10 *Hz*. In order to obtain reliable measurements, the specimens dimensions, $80 \times 2 \times 2$ mm, have been determined to have a ratio of 20 between the stiffness of the sample in the glassy state and the stiffness of the load cell. On this DMA apparatus, the load is directly measured using a load sensor and not determined from the actuating system. The compliance of the test set-up was taken into account for the determination of the viscoelastic properties. A sinusoidal tensile load was applied on the sample with a mean amplitude of 4 N and a peak-to-peak amplitude of 6 N, in order to test the specimen in the linear viscoelastic range.

4 Models for linear viscoelasticity

Linear viscoelasticity has been studied by many authors in the context of continuous mechanics. Historically, Caputo [10] proposed in 1971 a linear modeling of the dissipation taking into account the history of the solicitations applied to the material. Later, Ferry [22] and Lakes [28] proposed a framework on the basics of modeling viscoelastic behavior. This work has been enhanced by many contributions such as that of Lesieutre [30] in which the constitutive equations of viscoelasticity are formulated in the time domain based on a method called *"Anelastic Displacement Fields"* (ADF). A general objective of these works was to understand and model the physical phenomena before adapting the formulations to numerical simulation tools. Among others, Salençon [43] and Chevalier [12], propose some syntheses of the mechanical phenomena linked to viscoelasticity.

A viscoelastic material has a response that varies over time even if the loading it undergoes is constant over time. If the loading is carried out in stress and the response is observed in strain, one speaks of creep test. The reciprocal is called relaxation test. In addition, if a succession of loadings (in stress or strain) is applied to

the material then its final state corresponds to the sum of the modifications brought by each loading. The history of the loads applied to the viscoelastic material over time hence plays a major role in the behavior of the material, hence on the associated models required to describe it. The following constitutive law, which relates the stress tensor σ_{ij} to the strain tensor ε_{kl}, includes this dependency:

$$\sigma_{ij}(t) = C^{\infty}_{ijkl}\varepsilon_{kl}(t) + \int_0^t C^*_{ijkl}(t-\tau)\dot{\varepsilon}_{kl}(\tau)d\tau + C_{ijkl}(t)\varepsilon_{kl}(0) \qquad (1)$$

where $\sigma_{ij}(t) = C^{\infty}_{ijkl}\varepsilon_{kl}(t)$ corresponds to the elastic part of the constitutive law, C^{∞}_{ijkl} being the long-terme elasticity tensor. The tensor $C^*_{ijkl}(t)$ is called relaxation function and can be determined by measuring the evolution of the stress as a function of time when the material is subjected to a constant displacement. The rheological models used in viscoelasticity are typically built according to the assumptions made on the kernel of the relaxation function C^*_{ijkl}. The Fourier transform of this viscoelastic law is

$$\hat{\sigma}_{ij}(\omega) = C^{\infty}_{ijkl}\hat{\varepsilon}_{kl}(\omega) + j\omega\hat{C}^*_{ijkl}(\omega)\hat{\varepsilon}_{kl}(\omega), \qquad (2)$$

where $\hat{\ }$ corresponds to the Fourier transform and ω is the circular frequency. In order to simplify the writing for the introduction of the rheological models, in the following we restrict equations to the mono-dimensional case when the sample is subjected to a stress in tension. The constitutive law can then be written as

$$\hat{\sigma}(\omega) = E_{\infty}\hat{\varepsilon}(\omega) + j\omega\hat{E}^*(\omega)\hat{\varepsilon}(\omega) \qquad (3)$$

where E_{∞} represents the long-term elasticity modulus of the material for $t \to +\infty$ or $\omega \to 0$. This is classically written as

$$\hat{\sigma}(\omega) = E^*(\omega)\hat{\varepsilon}(\omega) \qquad (4)$$

where $E^*(\omega)$ is called Complex elastic modulus: in the frequency domain, linear viscoelastic problems can be solved as linear elastic problems with a complex modulus that depends on frequency. The real part of $E^*(\omega)$ is usually called storage modulus, its imaginary part being the loss modulus and the loss factor $\eta(\omega)$ being equal to the ratio between the imaginary and the real part of the complex modulus:

$$\eta(\omega) = \frac{\text{Im}(E^*(\omega))}{\text{Re}(E^*(\omega))}. \qquad (5)$$

4.1 Standard rheological models

Rheological models are classicaly used to define the frequency dependency of the complex modulus $E^*(\omega)$. The simplest model corresponds to constant values, which is called structural or hysteretic damping model:

$$E^* = E(1 + j\eta). \tag{6}$$

This corresponds to a very simple representation of the average viscoelastic behavior of the material. It is therefore generally used for lightly damped materials, such as metallic materials, that present a dissipated energy per cycle independent of the frequency when subjected to cyclic loading. The main drawback of this model is that it is non-causal which limits its use to the frequency domain [23]. Nevertheless, there is a way to make this model causal so that it can be used both in the frequency and time domain. The work carried out on the subject by Makris [35] leads to the formulation of a causal hysteretic model where the imaginary part is the same as that of the ideal hysteretic model:

$$E^*(\omega) = E(1 + j\eta\,\mathrm{sgn}(\omega)) \tag{7}$$

and where the real part is defined in order to make the model causal. Note that the ideal hysteretic model is equivalent to that expressed in Eq. (6) for positive frequencies.

In order to define a frequency dependency, rheological models have been historically built by combining simple mechanical elements like elastic springs and dampers. Figure 1 presents four standard rheological models commonly used in the literature.
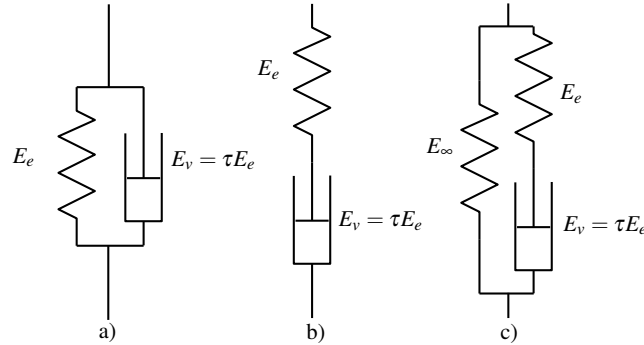

Fig. 1 Viscoelastic standard rheological models: a) Kelvin-Voigt b) Maxwell c) Zener

The Kelvin-Voigt model (Figure 1 (a)) is a simple model composed of a spring (with a stiffness E_e) and a damper (with a viscous damping constant E_v) in parallel. Its complex modulus is written as

$$E^*(\omega) = E_e + j\omega E_v. \tag{8}$$

It can be used as a first approximation to represent a viscoelastic behavior, event if the applicability is generally restricted to a narrow frequency band. In addition, this model is only suitable for low frequencies since the damping force tends to infinity

when the frequency increases.

The Maxwell model (Figure 1 (b)) is composed of a spring and a damper in series and the associated complex modulus can be expressed as

$$E^*(\omega) = E_e \frac{j\omega\tau}{1+j\omega\tau} \tag{9}$$

where $\tau = E_v/E_e$ is the relaxation time. This model can be used to describe the viscoelastic behavior but it is only applicable for a reduced frequency range as for the Kelvin-Voigt model and is not realistic at low frequency since it does not include a pure elastic component.

The Zener model, also named Standard Linear Solid model (Figure 1 (c)) represents a first realistic approximation of the viscoelastic behavior. Its complex modulus can be written as

$$E^*(\omega) = \frac{E_\infty + E_0 j\omega\tau}{1+j\omega\tau} \tag{10}$$

where E_0 corresponds to the instantaneous modulus of the material (*i.e.* when $t \to 0$ or $\omega \to +\infty$) and E_∞ corresponds to the long term modulus (*i.e.* when $t \to +\infty$ or $\omega \to 0$).

The three parameters of the Zener model may however be unsufficient to describe the complexity of the frequency-dependency of the viscoelastic properties for some materials. In this case, higher degree model may be used. Figure 2 illustrates the Generalized Maxwell Model (GMM) which is able to generate more complex evolutions of the viscoelastic behavior of materials. By combining N Maxwell cells in parallel, it is possible to accurately represent the experimental viscoelastic behavior over a wide band of frequency in dynamics thanks to a distribution of rational fractions shifted in frequency. The complex modulus associated with this model is written as

$$E^*(\omega) = E_\infty + \sum_{i=1}^{N} E_i \frac{j\omega\tau_i}{1+j\omega\tau_i} = E_\infty \left(1 + \sum_{i=1}^{N} \alpha_i \frac{j\omega\tau_i}{1+j\omega\tau_i}\right) \tag{11}$$

where E_i and τ_i represent the dynamic stiffness and the relaxation time of cell i. Up to the end of this chapter, the stiffening (or the dynamic stiffness ratio) is refered as $\alpha_i = E_i/E_\infty$. In addition, it may be noted that $E_0 = E_\infty + \sum_{i=1}^{N} E_i$.

At the price of an increase in the number of parameters that need to be identified, increasing the number of cells provides the ability of the model to describe more complex frequency dependencies (materials exhibiting several glass transitions for example).

The GMM may also be interpreted as a modelling strategy based on internal variables where the relaxation function $C_{ijkl}^*(t)$ is approximated by a Prony series development [46]. Numerous commercial software packages propose to take into account the viscoelastic behavior of a material by using Prony series: in the time
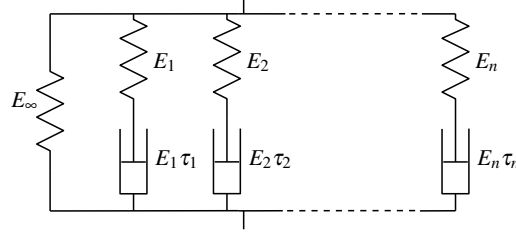
Fig. 2 Generalized Maxwell model

domain, one has

$$\sigma(t) = \int_{-\infty}^{t} E(t-s)\dot{\varepsilon}(s)ds, \tag{12}$$

with

$$E(t) = E_\infty + \sum_{i=1}^{N} E_i e^{-t/\tau_i}, \tag{13}$$

which is sometimes written as

$$E(t) = E_0 \left(1 - \sum_{i=1}^{N} \alpha'_i (1 - e^{-t/\tau_i}) \right) \tag{14}$$

where $\alpha'_i = \alpha_i/(1+\alpha_i)$, with $\alpha_i = E_i/E_\infty$ and $E_0 = E_\infty + \sum_{i=1}^{N} E_i$.

These one-dimensional rheological models are not sufficient to serve for 3D implementation, because of the couplings existing between the directions. However, the materials studied in this chapter being isotropic, the properties of the material are identical in the three directions of space. In this case, the tensor of the 3D viscoelastic constitutive law can be fully described with only two material characteristics. If we call this operator C^*_{ijkl}, such that

$$\hat{\sigma}_{ij}(\omega) = C^*_{ijkl}(\omega)\hat{\varepsilon}_{kl}(\omega) \tag{15}$$

then, C^*_{ijkl} may be written as

$$\hat{C}^*_{ijkl} = \frac{E^*(\omega)}{(1-2\nu)(1+\nu)} \begin{bmatrix} 1-\nu & \nu & \nu & 0 & 0 & 0 \\ \nu & 1-\nu & \nu & 0 & 0 & 0 \\ \nu & \nu & 1-\nu & 0 & 0 & 0 \\ 0 & 0 & 0 & \frac{1-2\nu}{2} & 0 & 0 \\ 0 & 0 & 0 & 0 & \frac{1-2\nu}{2} & 0 \\ 0 & 0 & 0 & 0 & 0 & \frac{1-2\nu}{2} \end{bmatrix} \tag{16}$$

where ν is the Poisson's ratio, which may also be frequency-dependent, even if its variation is of second order compared to the evolution of the modulus. Nevertheless, for some materials, it may be important to access to the frequency evolution of

v. The viscoelastic behavior of the shape memory polymers characterized in this chapter will be modeled by generalized Maxwell models.

4.2 Time-Temperature Superposition

As indicated above, the behavior of polymers is highly dependent on frequency, but is also highly dependent on temperature, this is particularly true for shape memory polymers. A lot of polymers behave, on specific temperature and frequency ranges, according to the Time-Temperature Superposition Principle [22], in particular in the glassy and rubbery states, together with the glass transition. This comes from the observation that temperature plays a role which is the opposite of frequency: an increase in frequency has the same effect as a decrease in temperature. This principle has been shown to be valid for a wide wariety of polymers but is not justified for polymer blends or composites. It can be interpreted as follows: considering a reference frequency evolution of the complex modulus $E^*(\omega, T_0)$ at a given temperature T_0, the frequency evolution of the complex modulus at another temperature T is

$$E^*(\omega, T) = E^*(a_T(T)\omega, T_0). \tag{17}$$

$E^*(\omega, T_0)$ is called the master curves. Hence, from a reduced set of measurements in frequency and temperature, the behavior of the materials can be described on larger ranges. Only the knowledge of the master curves and the shift factor $a_T(T)$ are required for this purpose. $a_T(T)\omega$ is usually called reduced frequency, it is identified by shifting in frequency the curves measured at temperature T to the ones measured at reference temperature T_0. Manual shifting is possible but automatic procedures are preferred [14, 42]. Several parametric models are available in literature to fit the temperature evolution of the shift factor. The Williams-Landel-Ferry (WLF) law [51], based on empirical data, is one of the most popular techniques. It consists in writing the shift factor as

$$\log(a_T(T)) = \frac{-C_1^0(T - T_0)}{C_2^0 + (T - T_0)}, \tag{18}$$

where C_1^0 and C_2^0 are two constants.
Another popular way to interpolate the value of the shift factor is the Arrhenius law [44]:

$$\log(a_T(T)) = \frac{E_a}{R}(\frac{1}{T} - \frac{1}{T_0}), \tag{19}$$

where E_a is the activation energy, $R = 8.314 \times 10^3$ kJ.mol^1.K^1 is the constant of perfect gas and T should be expressed in degree Kelvin. For a given material, the evolution of the shift factor may be fitted by one of these two equations (but may also be such that none of these models fits the experimental data).

In the following, the explicit dependency of the complex modulus to the temperature will be omitted (*ie* $E^*(\omega, T)$ will be identified to $E^*(\omega)$. The identification of the model parameters will be directly done on the master curves.

4.3 Identification of the parameters of the generalized Maxwell models

In this section, a method to identify the parameters of a generalized Maxwell model (GMM) representing the evolution of the mechanical behavior of the shape memory polymers is proposed. A hypothesis concerning the location of the $1/\tau_i$ poles of the GMM is formulated to facilitate its integration into computational routines in the frequency and time domains.

The identification of the parameters of a viscoelastic model requires the minimization of the difference between the measured and calculated storage and loss moduli, which is classically done using a least squares method. The real and imaginary part of the GMM can be separated by expressing respectively the storage module E' and the loss module E":

$$E^*(\omega) = E'(\omega) + jE"(\omega) \tag{20}$$

$$\text{with} \quad E'(\omega) = E_\infty + \sum_{i=1}^{N} E_i \frac{\omega^2 \tau_i^2}{1 + \omega^2 \tau_i^2} \tag{21}$$

$$\text{and} \quad E"(\omega) = \sum_{i=1}^{N} E_i \frac{\omega \tau_i}{1 + \omega^2 \tau_i^2} \tag{22}$$

A total of $2N + 1$ parameters to be identified from the master curves.

The identification of the parameters of a GMM can be conducted by an algorithm based on graphical methods such as those proposed by Dion [18]. These methods are based on a Pole-Zero formulation of the rheological model and make it possible to determine the number and the value of the Pole-Zero pairs which will be used for the construction of this model. Renaud [41] proposes to use these methods as initialization step then to add an optimization step in order to locate more accurately these couples and thus obtain a model which has a minimal number of cells.

In this chapter, another approach, used in [27], is used. Indeed, the poles of the GMM, which are $1/\tau_i$, are fixed by the user a priori. Such a constraint tends to increase the number of Maxwell cells needed to correctly represent the viscoelastic behavior but makes the identification problem easier to implement. On this basis, only the long-term modulus E_∞ and the dynamic moduli E_i have to be found, corresponding to only $N + 1$ unknowns. There is no precise rule to define the number of poles to use, but it seems that a distribution of three poles per decade with, at least, an additional decade beyond and above the frequency range of interest leads to confident results, and helps to stabilize the procedure at the same time. This approach is

preferred here since it is very easy to implement and provides good results in a very short time, at the price of a model order which is most of the time larger than the "optimal" one. Readers who are interested in finding lower order models can refer to [41].

The identification procedure consists in estimating the unknown parameters by solving in a least square sense the linear system

$$
\begin{bmatrix}
1 & \frac{\tau_1^2 \omega_1^2}{1+\tau_1^2 \omega_1^2} & \cdots & \frac{\tau_N^2 \omega_1^2}{1+\tau_N^2 \omega_1^2} \\
0 & \frac{\tau_1 \omega_1}{1+\tau_1^2 \omega_1^2} & \cdots & \frac{\tau_N \omega_1}{1+\tau_N^2 \omega_1^2} \\
\vdots & \vdots & \cdots & \vdots \\
1 & \frac{\tau_1^2 \omega_M^2}{1+\tau_1^2 \omega_M^2} & \cdots & \frac{\tau_1^2 \omega_M^2}{1+\tau_N^2 \omega_M^2} \\
0 & \frac{\tau_1 \omega_M}{1+\tau_1^2 \omega_M^2} & \cdots & \frac{\tau_N \omega_M}{1+\tau_N^2 \omega_M^2}
\end{bmatrix}
\begin{bmatrix}
E_\infty \\
E_1 \\
\vdots \\
E_N
\end{bmatrix}
=
\begin{bmatrix}
E'_{exp}(\omega_1) \\
E''_{exp}(\omega_1) \\
\vdots \\
E'_{exp}(\omega_M) \\
E''_{exp}(\omega_M)
\end{bmatrix}
\tag{23}
$$

where $\omega_1, \ldots, \omega_M$ are the M measured frequency points. The pseudo-inverse of the above matrix (whose size is $[2M, (N+1)]$) is required to obtain the values of E_∞ and E_i ($i = 1, \ldots, N$). It should be noted that in specific cases, some E_i parameters may be computed as negative values. In this kind of situation, it is necessary either to add new cells in the GMM, or to use a constrained minimization algorithm [9] to solve the following problem:

$$
\begin{cases}
\min_{E',E''} \sum_{i=1}^M \left(|E' - E'_{exp}(\omega_i)|^2 + |E'' - E''_{exp}(\omega_i)|^2 \right) \\
\text{with} \\
E_\infty \geqslant 0 \\
E_i \geqslant 0, i = 1, \ldots, N
\end{cases}
\tag{24}
$$

All the results presented hereafter use this strategy for the GMM identification.

5 Results

5.1 tBA/PEGDMA

Mechanical characterizations of the tBA/PEGDMA are already available in literature. Among others, the shape memory effect has been reported in [37], the recovery has been analyzed in [54], nano-indentation tests have been described in [52], while a dynamic mechanical analysis at 1 Hz has been reported in [39]. Nevertheless all these mechanical properties are not obtained for the same wt% components. The material used in this analysis has been deeply investigated in [7], the analysis covering large frequency and temperature ranges, but also several scales of characterization and several loading modes.

Figure 3 shows the whole set of measurements performed on the tBA/PEGDMA. The storage modulus E' varies from 0.7 MPa at low frequency, to 2200 MPa at high frequency, corresponding to a ratio of 3000 between the glassy modulus and the rubbery modulus. This impressive fall of the storage modulus at the glass transition state is accompanied by the rise of the loss factor η. Indeed the DMA results highlight very interesting tBA/PEGDMA viscoelastic properties: the value of the loss factor is higher than 1.5 in a wide range of frequencies and can reach a maximal value of 2.4. These values are particularly high, and this material has been used as a composite core which provides an extremely damped structure when the environmental conditions are close to the glass temperature [6].
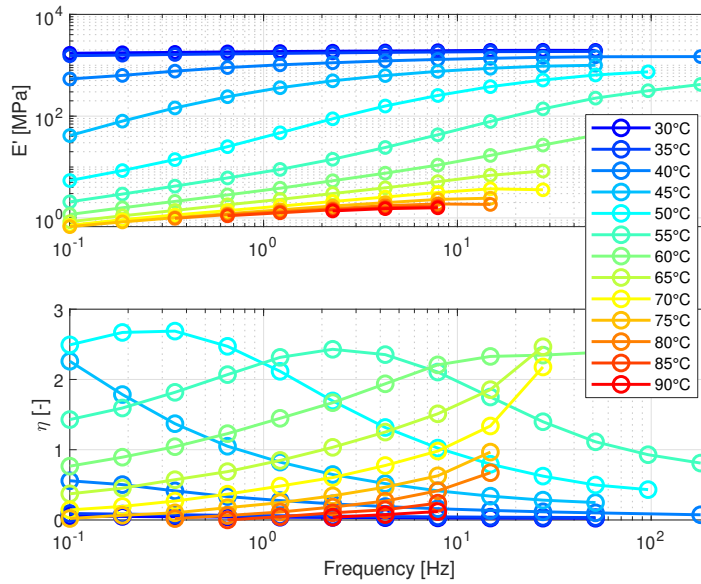

Fig. 3 DMA results on the tBA/PEGDMA.

Figure 4 shows the master curves. Except at very high temperature, the TTS works quite well. The shift factors are very well captured by the WLF law with $C_1 = 10.87$ and $C_2 = 32.57$ K, for a reference temperature $T_0 = 40°C$.

The results of the identification of the GMM model is shown in figure 5. The plots show the storage and loss moduli, and the loss factor. The crosses on the pictures correspond to the measured points coming from the DMA, after TTS according to WLF law. The GMM captures very well the behavior of the material on more than 12 decades, including the glassy and rubbery states, together with the glass transition. The numerical values of the cells components are provided in Appendix. In order to cover the 12 decades, a total of 42 cells have been used in the GMM. The total number of parameters is quite high compared to models like the 2S2P1D
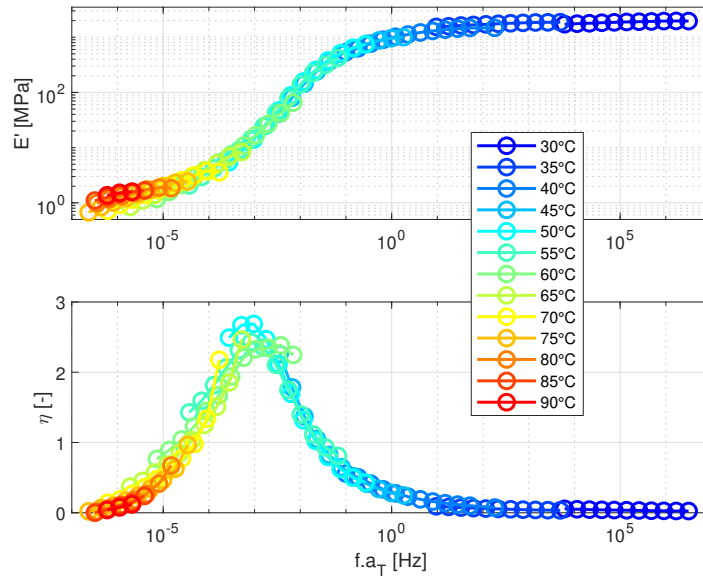
Fig. 4 Master curves of the storage modulus E' and the loss factor η according to the reduced frequency $f.a_T$ at a reference temperature $T_0 = 40°C$.

[38] already used for this material in [7], which requires only 7 parameters. The two models have almost the same precision in the frequency domain, however the GMM can be used for time computations, which is not the case of the 2S2P1D.
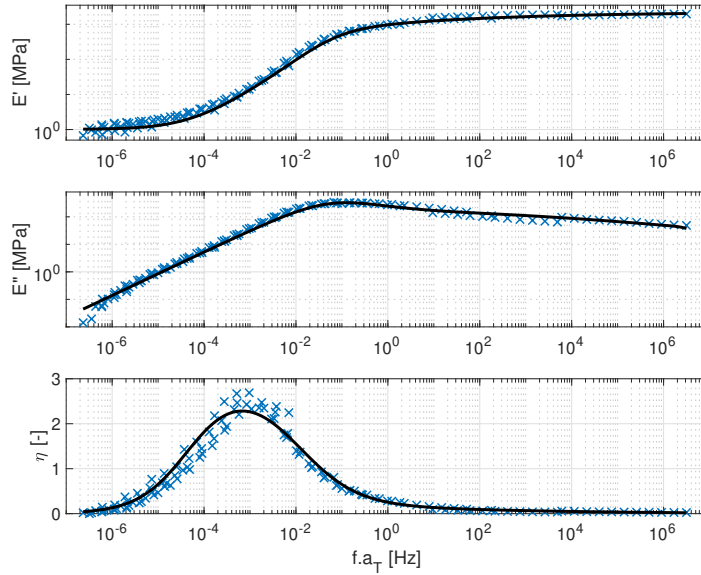
Fig. 5 Identification of the Generalized Maxwell Model for the tBA/PEGDMA at $T_0 = 40°C$ (solid lines: identified GMM; dots: measurement points).

5.2 SMP filament

Figure 6 shows the whole set of measurements performed on the SMP filament. The glass transition has been measured, the maximum value of the loss factor is about 1.5. Storage modulus has been measured around 4-5 MPa in the rubbery state, and around 1.5 GPa in the glassy state. The measurements at high temperature show a slight increase in the loss factor.

The TTS is also well verified on this material on the frequency and temperature ranges of interest. The master curves are shown in figure 10. Some discrepancies can be observed in the lower temperature range. The shift factors are well fitted by the WLF law with $C_1^0 = 9.66$, $C_2^0 = 55.9\ K$ and $T_0 = 58°C$.

As shown in figure 8, the GMM appears to be quite representative of the behavior of the SMP filament. The model fits well on the 13 decades of reduced frequencies. Only the loss factor at the glass transition is a little bit under-estimated by the model. The increase of loss factor at higher temperatures is also well captured by the GMM. Users of the model should we aware that the loss factor at very low frequency or very high temperature ($f.a_T < 2.7 \times 10^{-4}$) may be erroneous since no measurements have been done in this range where another physical phenomenon occurs. The numerical values of the model are provided in appendix.
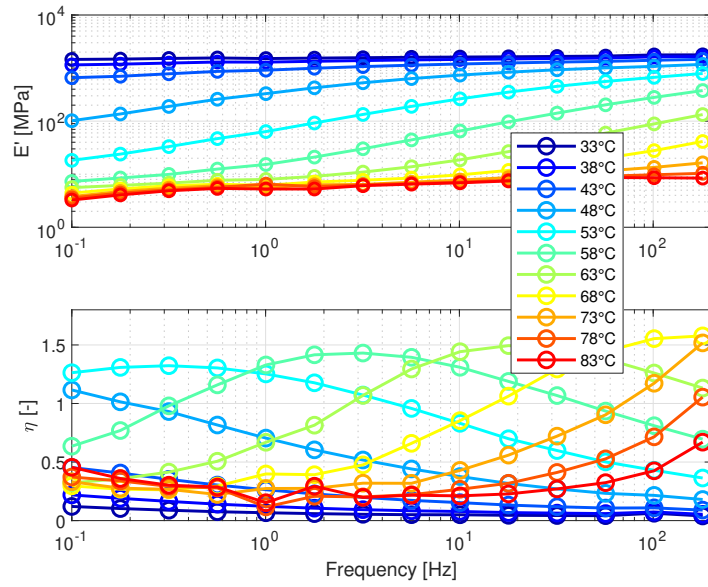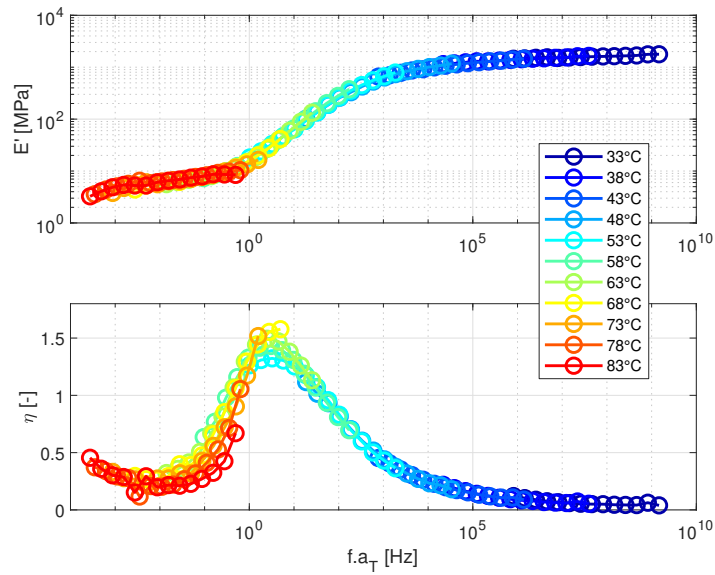
Fig. 6 DMA results on the SMP filament.
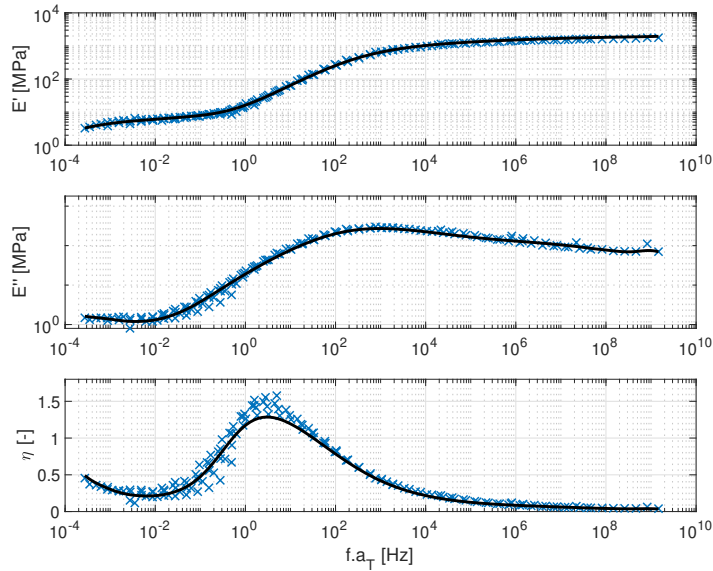

Fig. 7 Master curves of the SMP filament at $T_0 = 58°C$.

Fig. 8 Identification of the Generalized Maxwell Model for the SMP filament at $T_0 = 58°C$ (solid lines: identified GMM; dots: measurement points).

5.3 Vitrimer

Figure 9 shows the whole set of measurements performed on the hard network of vitrimer. The glass transition has been measured and the maximum value of the loss factor is about 0.72.

The TTS works quite well on this material on the frequency and temperature ranges of interest. The master curves are shown in figure 10. Some discrepancies can however be observed in the lower temperature range. The shift factors are well fitted by Arrhenius law with an activation energy $E_a = 1.70 \times 10^5$ J.mol^{-1}.K^{-1} and $T_0 = 46°C$. The GMM appears to be quite representative of the behavior of the vitrimer. As in the master curves, some difficulties appear in the zone corresponding to the lowest temperatures analyzed during the DMA tests. The GMM has some difficulties to fit the experimental data because in the glassy state, where the storage modulus stay constant, correspond to a loss factor which is not converging to zero as expected by the model: it seems that the vitrimer has a constant loss factor at low temperature. The numerical values of the model are provided in appendix, and users should be aware that the data provided should not be used for values outside the reduced frequency band $10^{-11} < f.a_T < 10$ Hz.
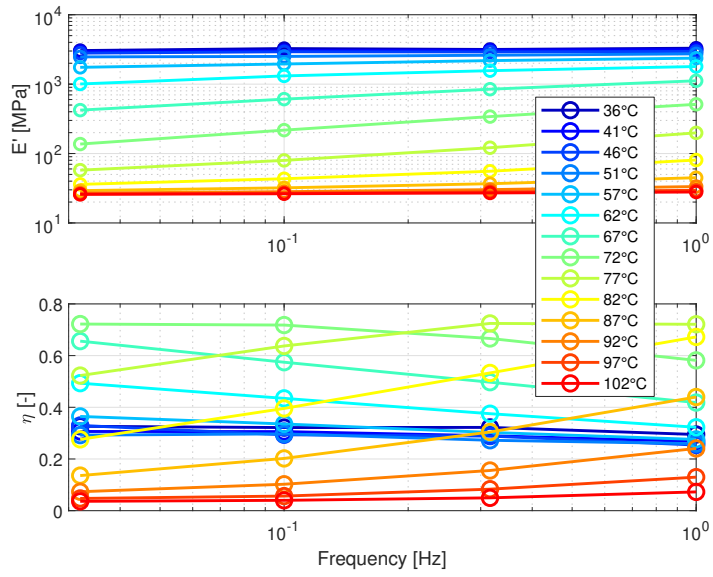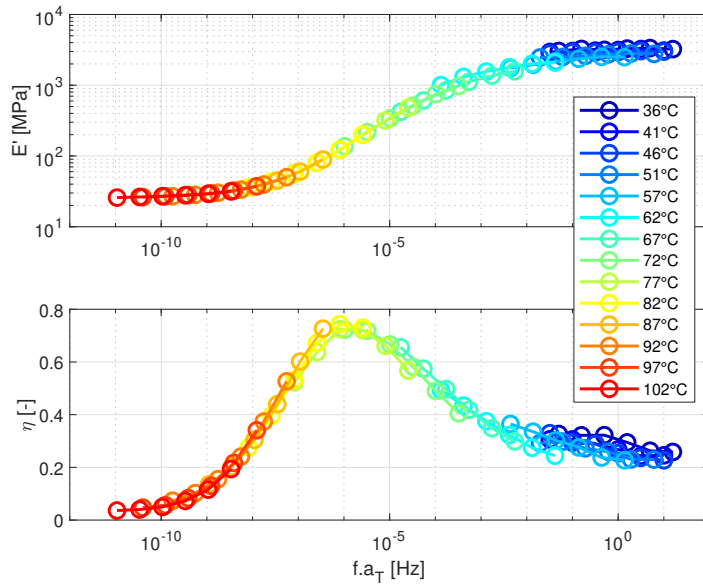
Fig. 9 DMA results on the hard network of vitrimer.

Fig. 10 Master curves of the hard network of vitrimer at $T_0 = 46°C$.

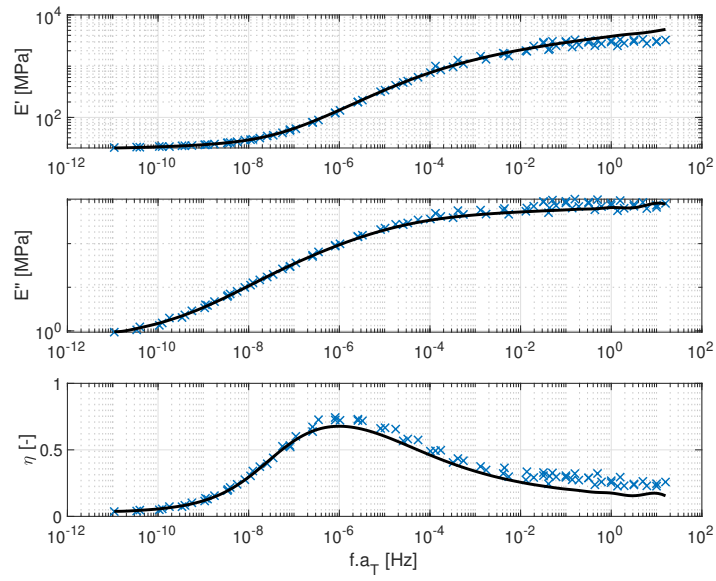**Fig. 11** Identification of the Generalized Maxwell Model for the hard network of vitrimer at $T_0 =$ 46°C (solid lines: identified GMM; dots: measurement points).

6 Conclusion

The viscoelastic properties of Shape Memory Polymers have been described and discussed in this chapter. An easy procedure for model identification has been presented and applied on the three materials which have been benchmarked. Starting from Dynamical Mechanical Thermal Analysis performed on reduced sets of frequencies and temperatures, the storage modulus and loss factor are measured. Then, the Time-Temperature Superposition has been used to identify the master curves. For the three materials, this principle is found to be representative of the measured behaviour. The shift factors are then fitted using either WLF or Arrhenius laws. Finally, a Generalized Maxwell Model has been used to describe the master curve, using a very simple identification procedure, which provides a model with 3 cells by decade. The complexity of the model is higher than the optimal one, but still representative of the behavior of the material on wide frequency and temperature ranges. For the three materials, the model is found to be effective on more than 11 decades. All numerical values are provided to the readers, hence anyone can use these models which are in accordance with the measurements performed on the three materials of interest. Among others, these models may be used to describe the shape memory effect in the time domain [21] or to describe the mechanical properties of composite structures embedding Shape Memory Polymers for vibration control in the frequency domain [6]. Users should be aware that the identified models should only be used in the reduced frequency range which has been considered for the fitting: out of this range, they could no longer be representative of the physical behavior. Typical illustrations are the behavior of the Vitrimer, which keeps a high loss factor at low temperature, or the SMP filament, having an increase of the loss factor at high temperatures.

Appendix - Numerical values of the GMM for the master curve of tBA/PEGDMA

Cell Id (i)	∞	1	2	3	4	5
τ_i [s^{-1}]	0	6.3559×10^{-8}	1.0593×10^{-7}	3.1780×10^{-7}	7.2089×10^{-7}	1.6353×10^{-6}
E_i [MPa]	0.97769	47.494	12.824	36.857	25.597	38.480
6	7	8	9	10	11	12
3.7094×10^{-6}	8.4144×10^{-6}	1.9087×10^{-5}	4.3297×10^{-5}	9.8215×10^{-5}	0.00022279	0.00050538
35.509	44.348	45.331	51.465	54.857	60.001	63.611
13	14	15	16	17	18	19
0.0011464	0.0026005	0.0058989	0.013381	0.030354	0.068854	0.15619
68.674	72.789	77.466	82.927	90.182	100.64	117.60
20	21	22	23	24	25	26
0.35430	0.80368	1.8231	4.1354	9.3808	21.279	48.270
147.41	195.49	236.00	181.53	88.156	38.936	17.638
27	28	29	30	31	32	33
109.50	248.38	563.42	1278.1	3149.0	7758.6	19116
8.4675	4.2157	2.0917	1.1444	0.59268	0.28032	0.13926
34	35	36	37	38	39	40
47100	1.1605×10^{5}	2.8593×10^{5}	7.0448×10^{5}	1.7357×10^{6}	4.2766×10^{6}	1.2830×10^{7}
0.067803	0.032689	0.017485	0.0050210	0.0028528	0.0049602	0.013080
41						
2.1383×10^{7}						
0.021141						

Appendix - Numerical values of the GMM for the master curve of SMP filament

Cell Id (i)	∞	1	2	3	4	5
τ_i [s^{-1}]	0	1.3656×10^{-10}	6.8280×10^{-10}	1.5076×10^{-9}	3.3288×10^{-9}	7.3499×10^{-9}
E_i [MPa]	0.00041175	122.25	27.421	46.242	31.513	57.238
6	7	8	9	10	11	12
1.6228×10^{-8}	3.5832×10^{-8}	7.9117×10^{-8}	1.7469×10^{-7}	3.8571×10^{-7}	8.5164×10^{-7}	1.8804×10^{-6}
46.875	62.971	58.318	66.349	68.579	73.597	81.764
13	14	15	16	17	18	19
4.1519×10^{-6}	9.1673×10^{-6}	2.0241×10^{-5}	4.4693×10^{-5}	9.8681×10^{-5}	0.00021789	0.00048109
91.310	100.64	121.28	127.62	153.02	151.15	152.60
20	21	22	23	24	25	26
0.0010622	0.0023454	0.0051786	0.011434	0.025247	0.055744	0.12308
123.22	90.911	58.486	35.484	20.420	11.493	6.0686
27	28	29	30	31	32	33
0.27176	0.60005	1.3249	2.9254	6.4592	14.262	31.490
3.2138	1.3316	0.87233	0.46338	0.63790	0.32339	0.65854
34	35	36	37	38	39	40
69.529	153.52	338.97	748.43	1652.5	3648.8	18244
0.24972	0.86167	0.87394	0.00047364	2.6729	0.66321	0.00059484

Appendix - Numerical values of the GMM for the master curve of Vitrimer

Cell Id (i)	∞	1	2	3	4	5
τ_i [s^{-1}]	0	0.012689	0.063445	0.14123	0.31438	0.69983
E_i [MPa]	10.806	1517.2	9.9502	790.00	0.049548	500.70

6	7	8	9	10	11	12
1.5579	3.4678	7.7195	17.184	38.252	85.151	189.55
203.33	345.30	251.11	289.77	249.72	254.53	229.18

13	14	15	16	17	18	19
421.94	939.26	2090.8	4654.3	10361.	23063.	51339.
217.72	193.13	171.00	142.87	115.73	88.780	65.993

20	21	22	23	24	25	26
1.1428×10^5	2.5440×10^5	5.6630×10^5	1.2606×10^6	2.8062×10^6	6.2466×10^6	1.3905×10^7
47.155	33.193	22.616	15.297	9.7769	6.3134	3.8148

27	28	29	30	31	32	33
3.0954×10^7	6.8904×10^7	1.5338×10^8	3.4144×10^8	7.6005×10^8	1.6919×10^9	3.7662×10^9
2.6396	1.6391	1.3584	0.83093	0.87719	0.46957	0.69845

34	35	36	37	38		
8.3838×10^9	1.8663×10^{10}	4.1544×10^{10}	9.2478×10^{10}	4.6239×10^{11}		
0.41526	0.00059210	0.0012208	0.0050371	14.355		

References

1. Araujo, A., Soares, C.M., Soares, C.M., Herskovits, J.: Optimal design and parameter estimation of frequency dependent viscoelastic laminated sandwich composite plates. Composite Structures **92**(9), 2321 – 2327 (2010)
2. Barwood, M.J., Breen, C., Clegg, F., Hammond, C.L.: The effect of organoclay addition on the properties of an acrylate based, thermally activated shape memory polymer. Applied Clay Science **102**, 41–50 (2014)
3. Berthelot, J.M., Assarar, M., Sefrani, Y., Mahi, A.E.: Damping analysis of composite materials and structures. Composite Structures **85**(3), 189 – 204 (2008)
4. Biju, R., Nair, C.R.: Synthesis and characterization of shape memory epoxy-anhydride system. Journal of Polymer Research **20**(2), 1–11 (2013)
5. Billon, K., Ouisse M. Sadoulet-Reboul, E., Collet, M., Butaud, P., Chevallier, G., Khelif, A.: Design and experimental validation of a temperature-driven adaptive phononic crystal slab. Smart Materials and Structures (2019). DOI 10.1088/1361-665X/aaf670
6. Butaud, P., Foltête, E., Ouisse, M.: Sandwich structures with tunable damping properties: on the use of shape memory polymer as viscoelastic core. Composite Structures **153**, 401–408 (2016). DOI 10.1016/j.compstruct.2016.06.040
7. Butaud, P., Ouisse, M., Placet, V., Renaud, F., Travaillot, T., Maynadier, A., Chevallier, G., Amiot, F., Delobelle, P., Foltête, E., Rogueda-Berriet, C.: Identification of the viscoelastic properties of the tBA/PEGDMA polymer from multi-loading modes conducted over a wide frequency–temperature scale range. Polymer Testing (2018). DOI 10.1016/j.polymertesting.2018.05.030
8. Butaud, P., Placet, V., Ouisse, M., Foltete, E., Gabrion, X.: Investigations on the frequency and temperature effects on mechanical properties of a shape memory polymer (veriflex). Mechanics of Materials **87**, 50–60 (2015). DOI 10.1016/j.mechmat.2015.04.002

9. Byrd, R.H., Gilbert, J.C., Nocedal, J.: A trust region method based on interior point techniques for nonlinear programming. Meathematical Programming **89**(1), 149–185 (2000)

10. Caputo, M., Mainardi, F.: Linear models of dissipation in anelastic solids. La Rivista del Nuovo Cimento (1971-1977) **1**(2), 161–198 (1971)

11. Chen, Y.C., Lagoudas, D.C.: A constitutive theory for shape memory polymers. part i: large deformations. Journal of the Mechanics and Physics of Solids **56**(5), 1752–1765 (2008)

12. Chevalier, Y., Tuong, J.V.: Mechanics of viscoelastic materials and wave dispersion. Iste (2010)

13. Chun, B.C., Cha, S.H., Chung, Y.C., Cho, J.W.: Enhanced dynamic mechanical and shape-memory properties of a poly (ethylene terephthalate)–poly (ethylene glycol) copolymer crosslinked by maleic anhydride. Journal of applied polymer science **83**(1), 27–37 (2002)

14. Dealy, J., Plazek, D.: Time-temperature superposition-a users guide. Rheol. Bull **78**(2), 16–31 (2009)

15. Diani, J., Gilormini, P.: On necessary precautions when measuring solid polymer linear viscoelasticity with dynamic analysis in torsion. Polymer Testing **63**, 275–280 (2017)

16. Diani, J., Gilormini, P., Agbobada, G.: Experimental study and numerical simulation of the vertical bounce of a polymer ball over a wide temperature range. Journal of Materials Science **49**(5), 2154–2163 (2014)

17. Diani, J., Gilormini, P., Frédy, C., Rousseau, I.: Predicting thermal shape memory of crosslinked polymer networks from linear viscoelasticity. International Journal of Solids and Structures **49**(5), 793–799 (2012)

18. Dion, J., Vialard, S.: Identification or rubber shock absorber mounts. Mécanique industrielle et matériaux **50**(5), 232–237 (1997)

19. Ege, K., Roozen, N., Leclere, Q., Rinaldi, R.G.: Assessment of the apparent bending stiffness and damping of multilayer plates; modelling and experiment. Journal of Sound and Vibration **426**, 129–149 (2018)

20. Ellson, G., Di Prima, M., Ware, T., Tang, X., Voit, W.: Tunable thiol–epoxy shape memory polymer foams. Smart Materials and Structures **24**(5), 055,001 (2015)

21. Fang, C., Leng, J., Sun, H., Gu, J.: A multi-branch thermoviscoelastic model based on fractional derivatives for free recovery behaviors of shape memory polymers. Mechanics of Materials **120**, 34–42 (2018)

22. Ferry, J.D., Ferry, J.D.: Viscoelastic properties of polymers. John Wiley & Sons (1980)

23. Gaul, L., Klein, P., Kemple, S.: Damping description involving fractional operators. Mechanical Systems and Signal Processing **5**(2), 81–88 (1991)

24. Grootenhuis, P.: The control of vibrations with viscoelastic materials. Journal of Sound and Vibration **11**(4), 421–433 (1970)

25. Hu, J., Chen, W., Fan, P., Gao, J., Fang, G., Cao, Z., Peng, F.: Epoxy shape memory polymer (smp): Material preparation, uniaxial tensile tests and dynamic mechanical analysis. Polymer Testing **62**, 335 – 341 (2017)

26. Hutcheson, S., McKenna, G.: In: 6th International Conference on Mechanics of Time Dependent Materials Conference, Monterey, California (2008)

27. Jaboviste, K., Sadoulet-Reboul, E., Peyret, N., Arnould, C., Collard, E., Chevallier, G.: On the compromise between performance and robustness for viscoelastic damped structures. Mechanical Systems and Signal Processing **119**, 65–80 (2019)

28. Lakes, R.S.: Viscoelastic solids, vol. 9. CRC press (1998)

29. Leibler, L., Montarnal, D., Tournilhac, F.G., Capelot, M.: Thermoset/supramolecular hybrid composites and resins that can be hot-formed and recycled (2016). US Patent 9,359,467

30. Lesieutre, G., Bianchini, E.: Time domain modeling of linear viscoelasticity using anelastic displacement fields. Journal of Vibration and Acoustics **117**(4), 424–430 (1995)

31. Li, J., Narita, Y.: The effect of aspect ratios and edge conditions on the optimal damping design of thin soft core sandwich plates and beams. Journal of Vibration and Control p. 1077546312463756 (2012)

32. Li, Y., Liu, Z.: A novel constitutive model of shape memory polymers combining phase transition and viscoelasticity. Polymer **143**, 298–308 (2018)

33. Lifshitz, J., Leibowitz, M.: Optimal sandwich beam design for maximum viscoelastic damping. International Journal of Solids and Structures **23**(7), 1027–1034 (1987)
34. Lin, J., Chen, L.: Shape-memorized crosslinked ester-type polyurethane and its mechanical viscoelastic model. Journal of applied polymer science **73**(7), 1305–1319 (1999)
35. Makris, N.: Causal hysteretic element. Journal of engineering mechanics **123**(11), 1209–1214 (1997)
36. Montarnal, D., Capelot, M., Tournilhac, F., Leibler, L.: Silica-like malleable materials from permanent organic networks. Science **334**(6058), 965–968 (2011)
37. Nair, D.P., Cramer, N.B., Scott, T.F., Bowman, C.N., Shandas, R.: Photopolymerized thiol-ene systems as shape memory polymers. Polymer **51**(19), 4383–4389 (2010)
38. Olard, F., Di Benedetto, H.: General 2s2p1d model and relation between the linear viscoelastic behaviours of bituminous binders and mixes. Road materials and pavement design **4**(2), 185–224 (2003)
39. Ortega, A.M., Kasprzak, S.E., Yakacki, C.M., Diani, J., Greenberg, A.R., Gall, K.: Structure–property relationships in photopolymerizable polymer networks: Effect of composition on the crosslinked structure and resulting thermomechanical properties of a (meth) acrylate-based system. Journal of applied polymer science **110**(3), 1559–1572 (2008)
40. Rao, M.D.: Recent applications of viscoelastic damping for noise control in automobiles and commercial airplanes. Journal of Sound and Vibration **262**(3), 457 – 474 (2003)
41. Renaud, F., Dion, J.L., Chevallier, G., Tawfiq, I., Lemaire, R.: A new identification method of viscoelastic behavior: Application to the generalized maxwell model. Mechanical Systems and Signal Processing **25**(3), 991–1010 (2011)
42. Rouleau, L.: Modélisation vibro-acoustique de structures sandwich munies de matériaux visco-élastiques. Ph.D. thesis, Paris, CNAM (2013)
43. Salençon, J.: Viscoélasticité pour le calcul des structures. Editions Ecole Polytechnique (2009)
44. Seitz, J., Balazs, C.: Application of time-temperature superposition prin- ciple to long term engineering properties of plastic materials. Polymer Engineering & Science **8**(2), 151–160 (1968)
45. Seitz, J., Balazs, C.: Application of time-temperature superposition principle to long term engineering properties of plastic materials. Polymer Engineering & Science **8**(2), 151–160 (1968)
46. Simo, J.C., Hughes, T.J.: Computational inelasticity, vol. 7. Springer Science & Business Media (2006)
47. Srivastava, V., Chester, S.a., Anand, L.: Thermally actuated shape-memory polymers: Experiments, theory, and numerical simulations. Journal of the Mechanics and Physics of Solids **58**(8), 1100–1124 (2010)
48. Stark, W., Jaunich, M., McHugh, J.: Dynamic mechanical analysis (dma) of epoxy carbon-fibre prepregs partially cured in a discontinued autoclave analogue process. Polymer Testing **41**, 140–148 (2015)
49. Tandon, G., Goecke, K., Cable, K., Baur, J.: Durability assessment of styrene-and epoxy-based shape-memory polymer resins. Journal of Intelligent Material Systems and Structures **20**(17), 2127–2143 (2009)
50. Tsai, Y., Tai, C.h., Tsai, S.J., Tsai, F.J.: Shape memory effects of poly (ethylene terephthalate-co-ethylene succinate) random copolymers. European Polymer Journal **44**(2), 550–554 (2008)
51. Williams, M.L., Landel, R.F., Ferry, J.D.: The temperature dependence of relaxation mechanisms in amorphous polymers and other glass-forming liquids. Journal of the American Chemical Society **77**(14), 3701–3707 (1955)
52. Wornyo, E., Gall, K., Yang, F., King, W.: Nanoindentation of shape memory polymer networks. Polymer **48**(11), 3213–3225 (2007)
53. Xie, T., Rousseau, I.a.: Facile tailoring of thermal transition temperatures of epoxy shape memory polymers. Polymer **50**(8), 1852–1856 (2009). DOI 10.1016/j.polymer.2009.02.035
54. Yakacki, C.M., Shandas, R., Lanning, C., Rech, B., Eckstein, A., Gall, K.: Unconstrained recovery characterization of shape-memory polymer networks for cardiovascular applications. Biomaterials **28**(14), 2255 – 2263 (2007)

55. Zeng, H., Leng, J., Gu, J., Yin, C., Sun, H.: Modeling the strain rate-, hold time-, and temperature-dependent cyclic behaviors of amorphous shape memory polymers. Smart Materials and Structures (2018)
56. Zhao, Q., Qi, H.J., Xie, T.: Recent progress in shape memory polymer: New behavior, enabling materials, and mechanistic understanding. Progress in Polymer Science **49**, 79–120 (2015)